

Comparative study of first-principles approaches for effective Coulomb interaction strength U_{eff} between localized f -electrons: lanthanide metals as example

Bei-Lei Liu,^{1,2} Yue-Chao Wang,^{2,*} Yu Liu,^{2,†} Yuan-Ji Xu,³ Xin Chen,²
Hong-Zhou Song,² Yan Bi,^{4,5} Hai-Feng Liu,² and Hai-Feng Song²

¹*School of Mathematical Sciences, Beijing Normal University, Beijing 100875, China*

²*Laboratory of Computational Physics, Institute of Applied Physics and Computational Mathematics, Beijing 100088, China*

³*Institute for Applied Physics, University of Science and Technology Beijing, Beijing 100083, China*

⁴*Center for High Pressure Science and Technology Advanced Research, Beijing 100094, China*

⁵*National Key Laboratory for Shock Wave and Detonation Physics, Institute of Fluid Physics, CAEP, Mianyang 621900, China*

Since the correlation strength has key influence on the simulation of strongly correlated materials, many approaches have been proposed to obtain the parameters using first-principles calculation. However, the comparison of the different Coulomb strength from these approaches and investigation of the mechanism behind are still needed. Taking lanthanide metals as example, we research the factors which affect the effective Coulomb interaction strength U_{eff} by local screened Coulomb correction (LSCC), linear response (LR) and constrained random-phase approximation (cRPA) in VASP. The $U_{\text{eff}}^{\text{LSCC}}$ value increases from 4.75 eV to 7.78 eV, $U_{\text{eff}}^{\text{LR}}$ is almost stable at about 6.0 eV (except for Eu, Er and Lu), and $U_{\text{eff}}^{\text{cRPA}}$ shows a two-stage decreasing trend in light lanthanides and heavy lanthanides. To investigate these difference, we established a scheme to analyze coexistence and competition between the orbital localization and the screening effect. We find that LSCC and cRPA are dominated by the orbital localization and the screening effect respectively, while LR shows a balance of the competition between the two factors. Additionally, the performance of these approaches are influenced by different starting points from PBE and PBE+ U , especially for cRPA. All these results give useful knowledge for the U_{eff} of lanthanide materials, and similar analysis can also be used in the research of other correlation strength simulation approaches.

PACS numbers: 63.20.dk, 71.27.+a, 71.10.Fd, 71.20.Eh, 71.15.Mb

I. INTRODUCTION

In last decades, a class of elements with $3d$, $4f$ or $5f$ electrons and their compounds have attracted tremendous attention from both fundamental research and industrial applications¹⁻³. These systems exhibit many exotic properties, such as high-temperature superconductivity⁴, colossal magneto-resistive effect⁵. Such materials are called strongly correlated materials due to their strong electron-electron interaction^{6,7}. However, the widely used density functional theory (DFT)⁸ in conventional local density approximation (LDA)^{9,10} or generalized gradient approximation (GGA)¹¹ is not suitable for these materials since the spurious self-interaction¹²⁻¹⁵. Many *ab initio* methods developed for strongly correlated materials have been successfully used in the simulation for thermodynamic properties and electronic structure properties^{6,9,11,16}. Among them, the correction methods based on the onsite Hubbard model such as DFT+ U ¹⁷⁻¹⁹, DFT plus dynamic mean-field theory (DFT+DMFT)^{20,21} and DFT plus Gutzwiller projected variational wave function (DFT+Gutzwiller)^{22,23} are popular and effective. Despite their good performance, these methods still have many key problems in construction of a high-precision Hubbard model, mainly including: 1) the definition of correlation space, i.e., the choice of local projection^{14,24}; 2) the double counting item, which needs to be deducted from the DFT part, has no strict form²⁵⁻²⁷; and especially, 3) the correla-

tion strength between localized electrons, i.e. the Hubbard U which describes the on-site Coulomb interaction under a certain screening, and Hund exchange interaction parameter J ^{28,29}. The correlation strength can even lead to qualitative difference in material properties³⁰. In the isotropic form³¹, the correlation strength is directly expressed by the effective Coulomb interaction between localized electrons $U_{\text{eff}} \equiv U - J$.

In experiment, people usually estimated the U value through the positions of Hubbard bands in X-ray photoemission spectroscopy (XPS) and bremsstrahlung isochromat spectroscopy (BIS) data^{32,33}. However, the experiments is costly and difficult to perform under some extreme conditions. In the early simulation work, U_{eff} values were tuned by fitting of simulated properties to the experimental one, like band gap³⁴⁻³⁶. This approach is not applicable in cases where experimental data are lacking, reduces the predictive ability of the correction methods based on Hubbard model, and there may also have significant differences in U_{eff} values by using different reference properties for the same system.

In order to alleviate the above problems, many approaches based on the first-principles have been developed to simulate the strength of on-site Coulomb interaction. For example, 1) Herbst *et al.* evaluate Hubbard- U using Hartree-Fock calculation. However, this method is based on the atomic limit, which is not the systems we really care about³⁷. 2) Dederichs *et al.*³⁸ developed the constrained density functional theory (cDFT) approach

to calculate the energy difference by constructing electronic configurations. In this approach, localized electrons are treated as core electrons in the full-potential framework. 3) Later, Cococcioni *et al.*³⁹ extended the cDFT approach to the more efficient pseudopotential framework based on the linear response (LR) theory, and obtained the U_{eff} value through the perturbation-induced variation of the occupation number of localized electrons. 4) Aryasetiawan *et al.*⁴⁰ developed the constrained random-phase approximation (cRPA) method based on the multi-body perturbation theory. This method can calculate the frequency dependent U . It is generally considered as a calculation method involving physical effects comprehensively⁴¹, but the computational cost is relatively high, and there are uncertainties for many factors, such as screening channel. 5) Local screened Coulomb correction (LSCC) method is proposed by one of the authors Yue-Chao Wang and Hong Jiang in recent years⁴³. It has been used to simulate the Coulomb interaction of $5f$ -electrons in β -UH₃⁴² and systematically calculate the U value of $3d$ metal oxides⁴³. It gives a good performance in evaluating Hubbard- U with dramatically reduced computational cost.

The above approaches are based on different physical process and it has been noted that these approaches could give different U_{eff} value for the same system^{37,41}. Nawa *et al.*⁴⁴ considered that comparison of the absolute values of U_{eff} calculated by different methods may not be meaningful. However, comparison of the characteristics in different methods is important from the perspective of both theory and practice. The change of U_{eff} with atomic number can help us understand the characteristics of these methods. For example, Tesch *et al.*⁴¹ studied the change trend of U_{eff} value calculated by LR method for d -electron metals, and emphasized the rise of correlation strength caused by stronger localization of d orbitals. Qiu *et al.*³⁷ studied the trend of U_{eff} value calculated by LR method for actinide metals, and emphasized the screening effect caused by different structures and the electronic localization change, which related to the evolution atomic volume.

Lanthanide metals is typical strongly correlated series, their $4f$ -electrons shows stronger localization than $3d$ and $5f$, which is a good platform for exploring the characteristics of different methods. The correction methods based on Hubbard model have been widely used to simulate properties of lanthanide metals. To name a few, Harmon *et al.*⁴⁵ simulated Gd using LDA+ U with $U_{\text{eff}} = 6.0$ eV, obtained a correct description of the antiferromagnetic ground state. Mohanta *et al.*⁴⁶ simulated Gd-Lu using GGA+ U , showed that $U_{\text{eff}} = 6.8$ eV can obtain the structure and magnetic properties basically consistent with the measured data. And Lochter *et al.*⁴⁷ carried out DFT+DMFT simulation with $U = 7$ eV, the structural properties, magnetic properties and photoelectron spectra are in good agreement with the experiment. We note that there are also many works using the first-principles approaches to calculate the correlation strength of $4f$ -

electrons. Nilsson *et al.*⁴⁸ reported the calculation of cRPA- U value for Ce-Gd, and Moree *et al.*⁴⁹ carried out a self consistent calculation of combining LSDA+ U with cRPA for lanthanide metals. For cDFT/LR method on the U_{eff} value of lanthanide metals, the calculation results are scattered in different works. For example, Dederichs *et al.* calculated the U_{eff} value of Ce as an impurity atom using cDFT, Cococcioni *et al.*³⁹ calculated the U_{eff} value of Ce using the LR method, and Tao *et al.*⁵⁰ calculated the U_{eff} value of Gd₁₃ cluster. However, as far as we know, systematic calculation of U_{eff} values using cDFT/LR approach has not been performed before. The performance of LSCC on lanthanide metals will also be reported for the first time in this paper.

In this work, we systematically simulated the on-site Coulomb interaction between $4f$ -electrons of lanthanide metals using approaches LSCC, LR and cRPA. All these approaches could be performed in the popular Vienna Ab initio Simulation Package (VASP)^{51,52}. Comparison of the trend of U_{eff} calculated with atomic number are performed. In particular, we analyze the competition between the orbital localization and the screening effect to explain the different performance of U_{eff} . In addition, we detect the sensitivity of U_{eff} to initial electronic state by simulation.

The paper is organized as follows. In Sec.II, we introduce the methods and the parameter setting used in this work. In Sec.III, the results of effective Coulomb interaction values are exhibited, the analysis of orbital localization and screening effect is performed, and the performance of U_{eff} from different electronic states are compared. Finally, our conclusions are summarized in Sec.IV.

II. METHODOLOGY

A. Local screened Coulomb correction (LSCC) approach

LSCC approach calculate the on-site interaction between localized electrons through the screened Coulomb interaction in the form of Yukawa potential⁴³

$$v_{sr}(\mathbf{r}, \mathbf{r}') = \frac{e^{-\lambda|\mathbf{r}-\mathbf{r}'|}}{|\mathbf{r}-\mathbf{r}'|}, \quad (1)$$

where $\lambda = 2[\frac{3\rho}{\pi}]^{1/6}$ is the parameter characterizing screening strength in the Thomas-Fermi screening model. For real system, we adapt a density-weighted averaging scheme (see S-III type in Yue-Chao *et al.*⁴³)

$$\bar{\lambda} = \frac{\int_{\text{aug}} \lambda(\mathbf{r})\rho(\mathbf{r})d\mathbf{r}}{\int_{\text{aug}} \rho(\mathbf{r})d\mathbf{r}}, \quad (2)$$

where $\rho(\mathbf{r})$ is electron-density, $\lambda(\mathbf{r})$ is the local screening parameter. The result is obtained by weighted averaging $\lambda(\mathbf{r})$ within the augmentation region. Using (1), the

screened Slater integrals can be calculated by⁵³

$$U_{m_1, m_2, m_3, m_4} = \langle \phi_{l, m_1} \phi_{l, m_2} | v_{sr} | \phi_{l, m_3} \phi_{l, m_4} \rangle. \quad (3)$$

Then we deduce the parameter U and J as

$$U = \frac{1}{(2l+1)^2} \sum_{m_2=1}^{2l+1} \sum_{m_1=1}^{2l+1} U_{m_1, m_2, m_1, m_2} \quad (4)$$

$$J = U - \frac{1}{(2l+1)(2l)} \sum_{m_2=1}^{2l+1} \sum_{m_1=1}^{2l+1} [U_{m_1, m_2, m_1, m_2} - U_{m_1, m_2, m_2, m_1}]. \quad (5)$$

B. Linear response (LR) approach

In LR approach, the interaction parameter be calculated as the second derivative of the ground state total energy with respect to the local electron occupation number n^I in site I ³⁹. The effective electronic potential is perturbed by an external potential $\alpha^I |\phi_m^I\rangle \langle \phi_m^I|$ only acts on the localized orbitals with amplitude α^I . The second derivative of the total energy with respect to n^I equals to the inverse of response function

$$\chi_{I, I} = \frac{\delta n^I}{\delta \alpha^I}. \quad (6)$$

In actual calculation, the artificial response of non-interacting electron systems is not related to the electron interaction, thus need to be subtracted. The response function of this part χ_0 could be evaluated by performing a non-self-consistent DFT calculation keeping the charge density constant^{37,39}. The on-site interaction is given by

$$U_{\text{eff}}^I = (\chi_0^{-1} - \chi^{-1})_{I, I}. \quad (7)$$

C. Constrained random-phase approximation (cRPA) approach

The screened Coulomb interaction in the GW approximation is⁵⁴

$$W(\mathbf{r}, \mathbf{r}'; \omega) = \frac{v(\mathbf{r}, \mathbf{r}')}{1 - v(\mathbf{r}, \mathbf{r}')P(\mathbf{r}, \mathbf{r}'; \omega)} \quad (8)$$

where v is the bare Coulomb interaction, and P is the polarizability, calculated within the random phase approximation:

$$P(\mathbf{r}, \mathbf{r}'; \omega) = \sum_{\mathbf{k}n}^{\text{occ}} \sum_{\mathbf{k}'n'}^{\text{unocc}} \frac{\psi_{\mathbf{k}n}^*(\mathbf{r}) \psi_{\mathbf{k}'n'}(\mathbf{r}) \psi_{\mathbf{k}n}^*(\mathbf{r}') \psi_{\mathbf{k}'n'}(\mathbf{r}')}{\omega - \varepsilon_{\mathbf{k}'n'} + \varepsilon_{\mathbf{k}n} + i\eta} - \frac{\psi_{\mathbf{k}n}(\mathbf{r}) \psi_{\mathbf{k}'n'}^*(\mathbf{r}) \psi_{\mathbf{k}'n'}(\mathbf{r}') \psi_{\mathbf{k}n}^*(\mathbf{r}')}{\omega + \varepsilon_{\mathbf{k}'n'} - \varepsilon_{\mathbf{k}n} - i\eta}, \quad (9)$$

where η is a positive infinitesimal. In the constrained random-phase approximation (cRPA) approach, it assumes that the screening between localized electrons can be treated well in the Hubbard model, so only the screening between the rest part need to be considered in the calculation of Hubbard U ^{40,55}. According to the difference of orbital characteristics, the polarizability is divided into P_f the polarizability between localized electrons and the rest part P_r . The partially screened Coulomb interaction used to calculate U value in cRPA is in the form of similar to (8), but the polarizability P needs to be replaced as P_r .

$$W^{\text{cRPA}}(\mathbf{r}, \mathbf{r}'; \omega) = \frac{v(\mathbf{r}, \mathbf{r}')}{1 - v(\mathbf{r}, \mathbf{r}')P_r(\mathbf{r}, \mathbf{r}'; \omega)} \quad (10)$$

From W^{cRPA} , we could calculate the effective interaction matrix as⁴⁹

$$U_{m_1, m_2, m_3, m_4}(\omega) = \langle \phi_{l, m_1} \phi_{l, m_2} | W^{\text{cRPA}}(\omega) | \phi_{l, m_3} \phi_{l, m_4} \rangle, \quad (11)$$

and derive the parameter U and J by Eq.(4) and Eq.(5) at $\omega = 0$.

There are many schemes for the calculation of P_f when correlated electron bands are entangled^{48,56,57}. We use the disentanglement method proposed by Miyake *et al.*⁵⁶. We cannot choose the same orbitals as in LSCC and LR due to the current implementation of cRPA in the VASP code. We set a large energy window $[-20 \text{ eV}, 20 \text{ eV}]$ to construct maximally localized Wannier functions⁵⁸⁻⁶⁰ (MLWFs) close to the atomic orbitals.

D. Computational details

The effective Coulomb interaction strength U_{eff} are calculated for lanthanide metal (Ce-Yb) with fcc structure, whose lattice parameters set as the experimental values at room temperature, see the Appendix VI. All calculations have been performed using VASP^{51,52}. The projector augmented wave (PAW) pseudopotentials⁶¹ is used. For the detail of PAW parameters, see the Appendix VI. The f -electrons is treated as valence electrons. The Perdew-Burke-Ernzerhof (PBE)¹¹ functional is applied for all the calculation. We calculate U_{eff} values for all system in paramagnetic states. All the plane-wave energy cutoffs is set as 600 eV. A Monkhorst-Pack⁶² k-mesh of $8 \times 8 \times 8$ (the k-mesh in cRPA calculation is set as $4 \times 4 \times 4$, which meets a precision of 0.2 eV on U_{eff} value) is applied to assure converged results. The LR approach is performed on $2 \times 2 \times 2$ supercells. We use 100 bands in the calculation of the polarizability.

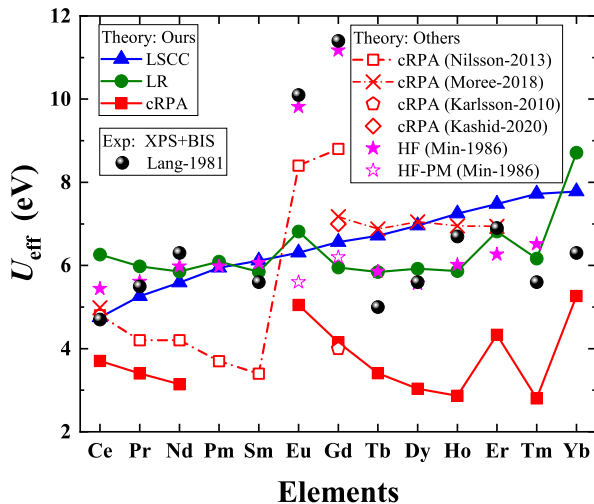


Fig. 1: The effective Coulomb interaction strength U_{eff} for lanthanide metals. The blue filled triangles represent the results obtained with LSCC approach, the green filled circles represent the results obtained with LR approach, and the red symbols represent the results obtained with cRPA approach (filled squares for this work, open squares for result by Nilsson *et al.*⁴⁸, cross for result by Moree *et al.*⁴⁹, pentagons for result by Karlsson *et al.*⁶³, and diamonds for Kashid *et al.*⁶⁴). The magenta symbols represent the results obtained with Hartree-Fock (HF) calculation (open stars for ferromagnetic states and filled stars for paramagnetic (PM) states by Min *et al.*⁶⁵, black filled balls for XPS and BIS experiments by Lang *et al.*³²).

III. RESULTS AND DISCUSSION

A. Trends of effective Coulomb interaction with different approaches

We present the effective Coulomb interaction U_{eff} derived by different first-principles approaches and other theoretical and experimental reference data in Fig.1. In the following, we denote the U_{eff} calculated by LSCC (or LR, cRPA) approach as $U_{\text{eff}}^{\text{LSCC}}$ (or $U_{\text{eff}}^{\text{LR}}$, $U_{\text{eff}}^{\text{cRPA}}$). Our calculations show that the U_{eff} values obtained by different approaches have different trends with the increasing of atomic number. Specially, $U_{\text{eff}}^{\text{LSCC}}$ increases from 4.75 eV to 7.78 eV with increasing atomic number. Except for Eu, Er and Yb, $U_{\text{eff}}^{\text{LR}}$ value is about 6.0 eV, with maximum variation of 0.26 eV. The $U_{\text{eff}}^{\text{LR}}$ value at Eu and Er is about 6.8 eV, and the $U_{\text{eff}}^{\text{LR}}$ value at Yb is significantly larger than others. The $U_{\text{eff}}^{\text{cRPA}}$ in this work shows two decreasing trends in light (Ce-Nd) and heavy (Eu-Ho) lanthanides, and also abruptly jumps in Eu, Er and Yb. $U_{\text{eff}}^{\text{cRPA}}$ is smaller than $U_{\text{eff}}^{\text{LSCC}}$ and $U_{\text{eff}}^{\text{LR}}$ in lanthanides. Some convergence problem occurred when we try to give enough virtual states for cRPA calculation. However, the lacking of the results of these two elements is not vital for our conclusion.

The value of $U_{\text{eff}}^{\text{LSCC}}$ and $U_{\text{eff}}^{\text{LR}}$ is in the range of previous empirical U , and is closer to the experimental estimate

and Hartree-Fock atomic calculation than $U_{\text{eff}}^{\text{cRPA}}$, except for Eu and Gd. We point out this difference may relate to the spin polarization. It is reported in the literature that the calculation results ignoring spin polarization effect are close to our results. Moreover, we note that the values with spin polarization are very large (about 10-12 eV), which may not be in the range that can simulate the properties in good agreement with the experiments. For $U_{\text{eff}}^{\text{cRPA}}$, the decreasing trend in light lanthanides also could be observed in the work of Nilsson *et al.*⁴⁸. However, the results of Eu and Gd in Nilsson *et al.*⁴⁸ is quite different with us. We note that the effect of spin polarization was also included in Nilsson *et al.*, and Gd- U_{eff} values reported in literatures have large difference due to different models and numerical methods in cRPA^{63,64}. Finally, we point out that the U_{eff} value in the work of Moree *et al.*⁴⁹, calculated by a self-consistent cRPA scheme combined with DFT+ U is generally larger, and does not show a obvious decreasing trend. We will discuss this phenomenon in Section III C.

Overall, similar performance of these approaches can be observed in both this work and many other reports. On one hand, it confirms that the approaches in this work are correctly used. On the other hand, the issue displayed in our results is general which may be encountered in other situations. Basing on the simulations above, analyses for the different characteristic between $U_{\text{eff}}^{\text{LSCC}}$, $U_{\text{eff}}^{\text{LR}}$ and $U_{\text{eff}}^{\text{cRPA}}$ are exhibited in the next section.

B. Characterization for localization of orbital and screening strength

In order to understand the trends of U_{eff} , we investigate the evolution of orbital localization and screening effect. From the definition, U_{eff} represents the on-site interaction between local electrons which are screened by the environment. Thus, the orbital localization of f -electrons and the screening strength of environment are two key factors should have influence on the U_{eff} . To understand the performance of different simulation approaches of U_{eff} , quantitative analysis of these two factors are of great importance.

Firstly, the orbital localization of f -electrons is shown in Fig.2. In Fig.2(a) the radial part of $4f$ -orbitals used in LSCC and LR approaches is shown. With the increase of atomic number, the f -electrons in real space becomes more localized. To quantitative characterize the orbital localization, the bare Coulomb interaction v is used, since localized electron distribution directly relates to a large v . The v of LSCC/LR and cRPA are shown in Fig.2(b). As the atomic number increases, v increases from 22.13 eV (23.51 eV for cRPA) to 35.40 eV (35.14 eV for cRPA). We note that bare Coulomb interaction of these two kinds of orbitals with difference less than 6 %, which indicates that the selected energy window gives a relatively good coherence between the atomic $4f$ orbitals and Wannier functions. To conclude, above results show that with the

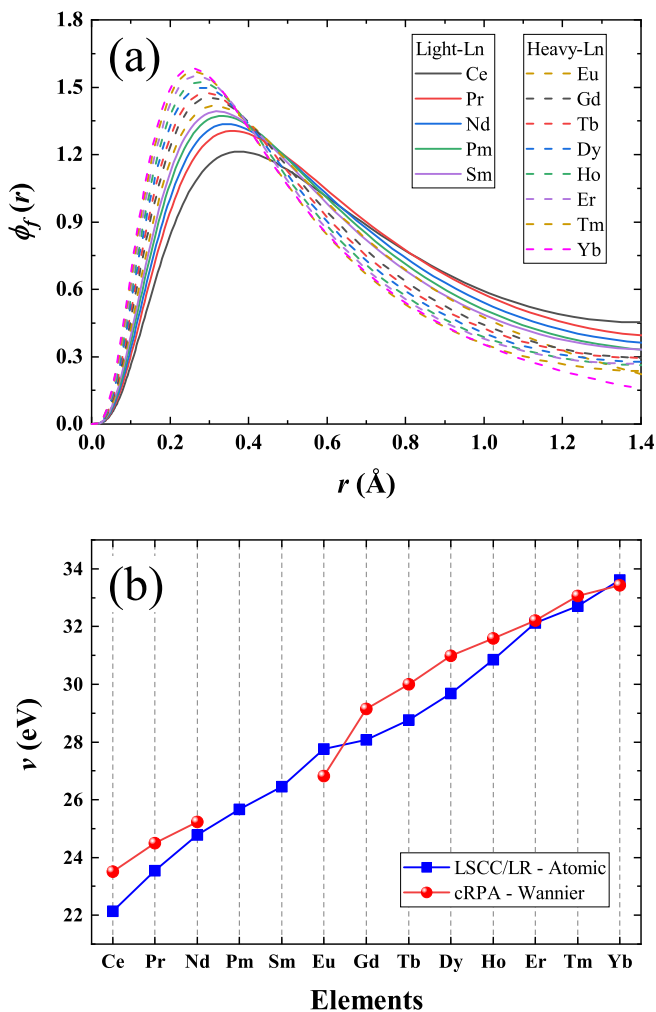


Fig. 2: (a) shows the radial 4f orbitals $\phi_f(r)$ of lanthanides in LSCC and LR approaches, the solid lines represent the light lanthanides, and chain lines represent heavy lanthanides. (b) shows the bare Coulomb interaction v of 4f orbitals in (a) and Wannier functions in cRPA approach, denoted as blue squares and red circles, respectively.

increase of atomic number, the localization of 4f-orbitals becomes stronger, which will lead to the increase of U_{eff} value.

Secondly, the screening strength is characterized in this work by the macroscopic dielectric constant $\varepsilon_{p,M} = \frac{v}{U_{\text{eff}}}$. It should be mentioned that the $\varepsilon_{p,M}$ differs from the real dielectric constant, since U_{eff} is the average interaction of on-site electrons, not the interaction at static limit. However, this definition can reflect screening effect from U_{eff} simulation approaches intuitively. As seen on Fig.3, the results of LSCC change little within the 4f elements, with slightly decrease of 0.5. $\varepsilon_{p,M}^{\text{LR}}$ shows an enhanced trend except for Eu, Er and Yb, with a variation less than 1.8. While $\varepsilon_{p,M}^{\text{cRPA}}$ is the largest in absolute value and changing amplitude, showing a two-stage enhanced trend in light and heavy lanthanides. Both $\varepsilon_{p,M}^{\text{LR}}$ and

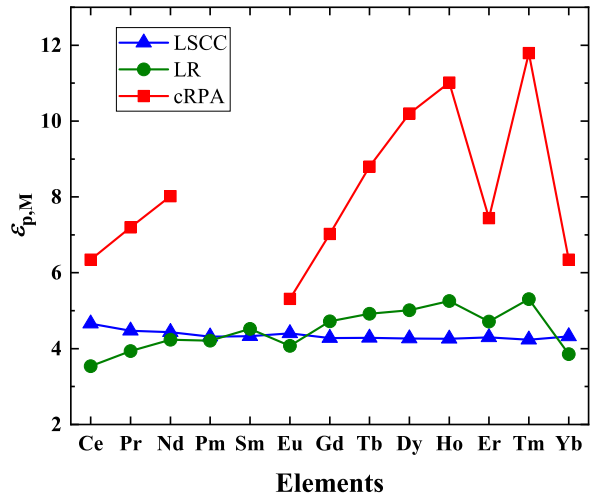


Fig. 3: The macroscopic dielectric constant $\varepsilon_{p,M} = \frac{v}{U_{\text{eff}}}$ of lanthanides. The blue triangles represent the results in LSCC approach, the green circles represent the results in LR approach, and the red squares represent the results in cRPA approach.

$\varepsilon_{p,M}^{\text{cRPA}}$ down suddenly in Eu, Er and Yb. These results show that the increasing trend of U_{eff} value in LSCC is dominated by the orbital localization. In cRPA method, the screening effect dominates the trend of U_{eff} , while the stable $U_{\text{eff}}^{\text{LR}}$ is the balance of competition between the orbital localization and screening effect.

For LSCC, the screening parameter λ depends on the charge density (see Eq.(2)). Based on Thomas-Fermi screening model, only the short-range metallic screening is considered in LSCC. Fig.4(a) shows that λ_{scf} gradually increases with the number of f -electrons, ranges from 1.50 to 2.12, where λ_{scf} denotes the screening parameter λ calculated by self-consistent charge density. λ can also be set manually. We report the macroscopic dielectric constant with respect to λ for different elements (with different f -localized orbital) in Fig.4(b). Larger λ led to the enhance of the short-range screening. However, the bare Coulomb interaction between correlated electrons is also enhanced at the same time. The macroscopic dielectric constant for LSCC is almost unchanged, and even slightly decrease, which is dominated by the correlated electrons.

For LR, we calculated the occupation number of bath electrons (i.e., the result of total occupation number deducting the f -electrons, $n_b = n_{\text{tot}} - n_f$), as plotted in Fig.5. With the increase of the radius of PAW augmented region (see AppendixVI), the occupation number of bath electrons gradually increases from Ce, but has three sharp drops in Eu, Er and Yb. The trend of n_b is same as $\varepsilon_{p,M}^{\text{LR}}$. LR approach is based on the perturbation-induced transfer of the occupation number, larger occupation number of bath electrons is likely to make charge transfer easier. However, the screening effect also depends on the correlated orbital, thus $\varepsilon_{p,M}^{\text{LR}}$

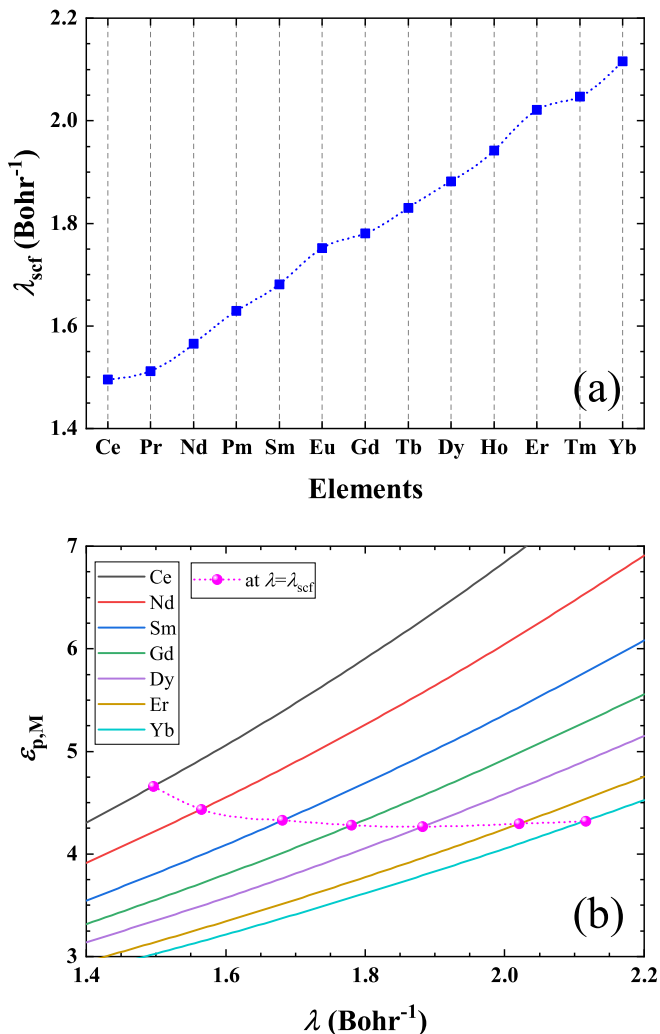


Fig. 4: (a) shows the screening parameter λ_{scf} (calculated with self-consistent charge density) of lanthanides in LSCC approach. (b) shows the variation of macroscopic dielectric constant with respect to λ (set manually) and elements. The magenta symbols represent λ_{scf} .

is not fully proportional to the occupation number of bath electrons n_b . For cRPA, the results are sensitive to the density of states, since cRPA is based on transition between occupied-unoccupied electronic states in several eV, as in Eq.(9). In the work of Nilsson *et al.*⁴⁸, it is noticed that the density of states of f -electrons near the Fermi energy increases with the $4f$ series, leading to the enhancement of the polarization effect of f and environmental electrons, and thus enhancing the screening. In our work, we also observed that the density of state of f -electrons near the Fermi energy increases with the filling f -shell. As an example, we showed the typical cases in Fig.6. Meanwhile, under the uniform electron gas limit, the polarizability is proportional to the charge density, thus the occupation number of bath electrons n_b is also affect the trend of $\epsilon_{\text{p,M}}^{\text{cRPA}}$. We point out that PBE

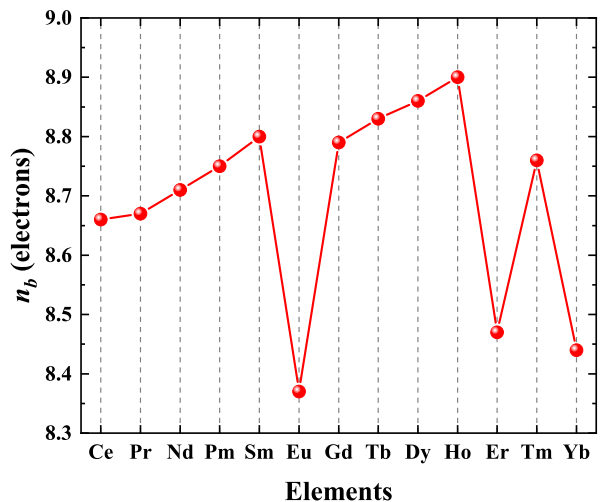


Fig. 5: The occupation number of bath electrons $n_b (= n_{\text{tot}} - n_f)$ of lanthanides.

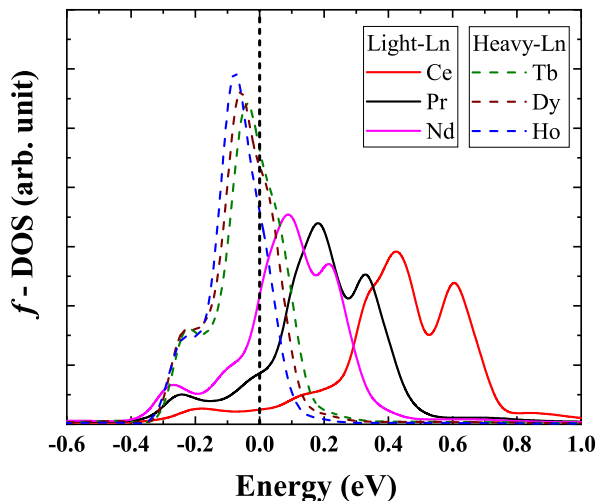


Fig. 6: Comparison of f density of states. The solid lines represent f -DOS of typical light lanthanides: Ce, Pr, Nd. The chain lines represent f -DOS of typical heavy lanthanides: Tb, Dy, Ho. The black vertical line represents Fermi level.

exchange-correlation functional cannot qualitatively calculate the electronic state of the strongly correlated system, which leads to excessive concentration of electronic states near the Fermi energy. This concentration of electronic states increases with the $4f$ series, which is one source of excessive decreasing $\epsilon_{\text{p,M}}^{\text{cRPA}}$. In the following section, we will simulate U_{eff} using electronic state from PBE + U .

C. Sensitivity of U_{eff} to initial electronic state

The simulations above are all based on the same initial electronic states, which is obtained from PBE. Since

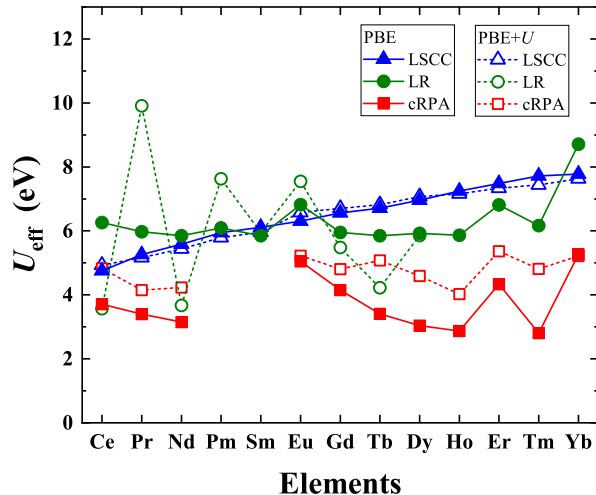


Fig. 7: Comparison of calculated U_{eff} value of of lanthanides with initial electronic states from PBE and PBE+ U ($U = 6.0$ eV). The filled symbols represent the results obtained with PBE electronic state, and open for the results obtained with PBE+ U electronic state.

PBE (together with other LDA and GGA functionals) is often believed not appropriate for strongly correlated materials, it is necessary to find out how these U simulation approaches perform in a more “reasonable” initial point. In Fig.7, the results calculated using PBE electronic states with the results calculated using PBE+ U ($U = 6.0$ eV) electronic states are compared. Using the PBE+ U electronic state, the $U_{\text{eff}}^{\text{cRPA}}$ is change dramatically (compare with $U_{\text{eff}}^{\text{cRPA}}$ using PBE electronic states), while the LSCC approach only change a little (maximum change of 0.278 eV). It could be observed that $U_{\text{eff}}^{\text{LR}}$ also has large variation except for Sm, but not monotonically.

We speculate that the decrease of the density of state of the f electron near the Fermi energy leads to the increase of $U_{\text{eff}}^{\text{cRPA}}$. Taking Ho as an example in Fig.8, we observed a significant decrease in the density of states of the f -electron near the Fermi energy when using PBE+ U . At Eu and Yb, the electronic state obtained by PBE+ U is still large near the Fermi energy, and the electronic state obtained by PBE is not large near the Fermi energy, respectively. Since the PBE+ U method mainly change the occupation number and the density of states, the localized orbital is almost unchanged, the behavior of cRPA and LSCC are consistent with the characteristics we analyzed earlier.

We note that the process of LR self-consistent calculation is different from the cRPA method⁶⁶. In the LR approach, the U value is taken as the coefficient for the correction of the total energy with respect to the number of electrons. Exact total energy varies linearly with respect to the number of electrons. In LDA/GGA, the number of electrons has a nonlinear contribution to the total energy, which is mainly as a quadratic term brought by the Hartree energy part. After correction, the U value

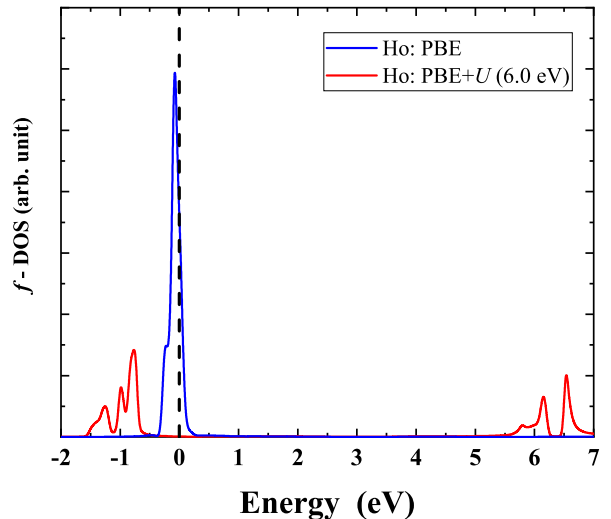


Fig. 8: Comparison of f density of states. The blue line represent f -DOS of Ho from PBE, and red line represent f -DOS of Ho from PBE+ U ($U = 6.0$ eV). The black vertical line represents Fermi level.

obtained by LR calculation will be reduced accordingly. However, the f electron orbitals are nearly degenerate in the standard $U = 0$ PBE calculation, perturbation is more likely to cause the variation of the occupations. While in PBE+ U calculation, the corresponding energy of filled and unfilled f -electrons near Fermi level become larger (e.g., see Fig.8), and the occupation is hard to change under the same perturbation.

Our results show remarkable variation between the U_{eff} from different initial electronic states especially in cRPA. It makes the understanding of the relation between DFT and the correction methods with U (such as DFT+ U) vital. If the methods like DFT+ U are treated as some self-interaction-correction methods to PBE or other functionals, one should take the U_{eff} from initial electronic state which is calculated by just by the functional to be corrected. If the DFT+ U is treated as a functionals which should be solved fully self-consistent including the U , the final U_{eff} is somehow calculated from a DFT+ U initial states. Obversely, these two kinds of interpretation could lead to much different results, as can be seen in this work. Since more and more works have taken self-consistency of U value with cRPA, this issue will becomes more crucial and deserves further investigation.

IV. CONCLUSION

In summary, in order to research the factors that affects the effective Coulomb interaction strength in different first-principles approaches, we systematically calculated U_{eff} for lanthanide metals using LSCC, LR and cRPA method, and investigated their different performance. It could be observed that the trend of U_{eff} values

TABLE I: Values of experimental fcc primitive cell volumes and radius of PAW augmented region for lanthanide metals.

Elements	Volumes (\AA^3)	PAW radius (\AA)
Ce	34.34	1.487
Pr	34.55	1.492
Nd	34.02	1.503
Pm	33.71	1.513
Sm	33.29	1.524
Eu	48.24	1.529
Gd	33.19	1.545
Tb	32.07	1.550
Dy	31.56	1.561
Ho	31.17	1.572
Er	30.67	1.386
Tm	30.09	1.487
Yb	41.91	1.498

(with filling f shell) has an obvious contrast between the three approaches. The $U_{\text{eff}}^{\text{LSCC}}$ value gradually increases, $U_{\text{eff}}^{\text{LR}}$ value is almost unchanged at about 6.0 eV, and $U_{\text{eff}}^{\text{cRPA}}$ shows a two-stage decreasing trend in light lanthanides and heavy lanthanides, with obvious change (1-2 eV) in lanthanides. Meanwhile, there are three abrupt jumps in Eu, Er, and Yb for both $U_{\text{eff}}^{\text{LR}}$ and $U_{\text{eff}}^{\text{cRPA}}$.

We analyzed these different trends based on the orbital localization and the screening effect. The rise of f -orbitals localization with increasing nuclear charge contributes to the increase of U_{eff} , while the screening effect also stronger in the light lanthanides and heavy lanthanides, respectively. The competition between the two factors is the main mechanism of the trends in different approaches. We conclude that the trend of LSCC is dominated by the localization of f -orbitals, while cRPA

is dominated by the screening effect, and $U_{\text{eff}}^{\text{LR}}$ is the balance of two factors. Additionally, the suddenly decrease of bath occupation number at Eu, Er and Yb is related to the sharp changes of $U_{\text{eff}}^{\text{LR}}$ and $U_{\text{eff}}^{\text{cRPA}}$.

In addition, we simulated the dependence of U_{eff} to electronic state. The result show that $U_{\text{eff}}^{\text{LR}}$ and $U_{\text{eff}}^{\text{cRPA}}$ are sensitive to electronic state, due to their stronger dependence on screening effect. Thus a self-consistent scheme for LR and cRPA is particularly important.

The behavior of different first-principles approaches for U_{eff} can be used to guide the choice of suitable U_{eff} parameter. Similar analysis can also be applied in other strongly correlated systems and other U_{eff} simulation approaches. Comparison of different first-principles approaches may provide a new perspective for the choice of Coulomb interaction strength in the future researches.

V. ACKNOWLEDGEMENT

We thank Hong Jiang, Hua-Jie Chen, Xing-Yu Gao, Jie Sheng, Bo Sun, Ming-Feng Tian, Jian-Zhou Zhao for helpful discussions. The work was supported by the National Nature Science Foundation of China (NO.U1930401, NO.12004048, NO.12204033, and NO.11971066), the National Key Research and Development Program of China (No.2021YFB3501503) and the Foundation of LCP. We thank the Tianhe platforms at the National Supercomputer Center in Tianjin.

VI. APPENDIX: VALUES OF VOLUME AND PAW PARAMETERS

The detail of experimental fcc primitive cell volumes at ambient pressure and temperature²¹, and radius of PAW augmented region for lanthanide metals be presented in Table I.

* Electronic address: yuechao.wang@126.com

† Electronic address: liu_yu@iapcm.ac.cn

¹ V. B. Grasso, Rare Earth Elements in National Defense: Background, Oversight Issues, and Options for Congress, in (Library Of Congress Washington DC Congressional Research Service, 2013).

² K. A. Gschneidner and J. L. Eyring, Metal, in Handbook on the Physics and Chemistry of Rare Earths, Vol. 1 (Elsevier, 1978), pp. 1-894.

³ J. J. Croat, J. F. Herbst, R. W. Lee, and F. E. Pinkerton, *J. Appl. Phys.* **1984**, 58, 2078.

⁴ Y. Kamihara, T. Watanabe, M. Hirano, and H. Hosono, *J. Am. Chem. Soc.* **2008** 130, 3296.

⁵ Y. Tokura, *Rep. Prog. Phys.* **2006** 69, 797.

⁶ V. Anisimov and Y. Izyumov, Electronic Structure of Strongly Correlated Materials (Springer-Verlag, Berlin Heidelberg, 2010).

⁷ A. Avella and F. Mancini, Strongly Correlated Systems. Theoretical Methods (Springer, Heidelberg; New York,

2012).

⁸ R. M. Martin, Electronic Structure: Basic Theory and Practical Methods (Cambridge University Press, Cambridge, UK ; New York, 2004)

⁹ J. P. Perdew and A. Zunger, *Phys. Rev. B* **1981**, 23, 5048-5079.

¹⁰ D. M. Ceperley, B. J. Alder, *Phys. Rev. Lett.* **1980**, 45, 566-569.

¹¹ J. P. Perdew, K. Burke, and M. Ernzerhof, *Phys. Rev. Lett.* **1996**, 77, 3865.

¹² N. Hamada, H. Sawada, and K. Terakura, Spectroscopy of Mott insulators and correlation metals, (Springer-Verlag, Berlin, 1995)

¹³ D. Sarma, N. Shanthi, S. Barman, N. Hamada, H. Sawada, and K. Terakura, *Phys. Rev. Lett.* **1995**, 75(6), 1126.

¹⁴ B. Amadon, F. Jollet, and M. Torrent, *Phys. Rev. B* **2008**, 77(15), 155104.

¹⁵ S. Y. Savrasov, and G. Kotliar, *Phys. Rev. Lett.* **2000**, 84(16), 3670(4).

- ¹⁶ M. Casadei, X. Ren, P. Rinke, A. Rubio, and M. Scheffler *Phys. Rev. B* **2016** 93, 075153.
- ¹⁷ V. I. Anisimov, J. Zaanen, and O. K. Andersen, *Phys. Rev. B* **1991**, 44, 943.
- ¹⁸ V. I. Anisimov, F. Aryasetiawan, and A. I. Lichtenstein, *J. Phys. Condens. Matter* **1997**, 9, 767.
- ¹⁹ B. Himmetoglu, A. Floris, S. de Gironcoli, and M. Cococcioni, *Int. J. Quantum Chem.* **2014**, 114, 14.
- ²⁰ G. Kotliar, S. Y. Savrasov, K. Haule, V. S. Oudovenko, O. Parcollet, and C. A. Marianetti, *Rev. Mod. Phys.* **2006**, 78, 865.
- ²¹ A. K. McMahan, R. T. Scalettar and M. Jarrell, *Phys. Rev. B* **2009**, 80, 235105.
- ²² X. Deng, X. Dai, and Z. Fang, *EPL Europhys. Lett.* **2008**, 83, 37008.
- ²³ N. Lanat'a, Y. Yao, C.-Z. Wang, K.-M. Ho, and G. Kotliar, *Phys. Rev. X* **2015**, 5, 011008.
- ²⁴ A. B. Shick, A. I. Lichtenstein, and W. E. Pickett, *Phys. Rev. B* **1999**, 60, 10763.
- ²⁵ Y.-C. Wang, Z.-H. Chen, and H. Jiang, *J. Chem. Phys.* **2016**, 144, 144106.
- ²⁶ M. T. Czyzyk and G. A. Sawatzky, *Phys. Rev. B* **1994**, 49, 14211.
- ²⁷ S. Rye and M. J. Han, *Sci. Rep.* **2018**, 8, 9559 (2018).
- ²⁸ H. Jiang, P. Rinke and M. Scheffler, *Phys. Rev. B* **2012**, 86, 125115.
- ²⁹ L. Wang, T. Maxisch, and G. Ceder, *Phys. Rev. B* **2006**, 73, 195107.
- ³⁰ S. Eryigit, C. Parlak, and R. Eryigit, *J. Phys.: Condens. Matter* **2022**, 17, 34(29).
- ³¹ S. Dudarev, G. Botton, S. Savrasov, C. Humphreys, *Phys. Rev. B* **1998**, 57, 1505.
- ³² J.K. Lang, Y. Baerand and P.A. Cox, *J. Phys.F* **1981**, 11, 121.
- ³³ T. Kaurila, J. Väyrynen, and M. Isokallio, *J. Phys.: Condens. Matter* **1997**, 9, 6533.
- ³⁴ O. Bengone, M. Alouani, P. Blöchl, and J. Hugel. *Phys. Rev. B* **2000**, 62, 16392.
- ³⁵ C. W. M. Castleton, J. Kullgren, and K. Hermansson. *J. Chem. Phys.* **2007** 127, 244704.
- ³⁶ J. T. Pegg, X. Aparicio-Anglès, M. Storr, and N. H. de Leeuw. *J. Nucl. Mater.* **2017** 492, 269.
- ³⁷ R. Qiu, B. Ao and L. Huang *Comput. Mater. Sci.* **2020**, 171, 109270.
- ³⁸ P. H. Dederichs, S. Blügel, R. Zeller, and H. Akai, *Phys. Rev. Lett.* **1984**, 53, 2512.
- ³⁹ M. Cococcioni and S. de Gironcoli, *Phys. Rev. B* **2005**, 71, 035105.
- ⁴⁰ F. Aryasetiawan, M. Imada, A. Georges, G. Kotliar, S. Biermann, and A. I. Lichtenstein, *Phys. Rev. B* **2004**, 70, 195104.
- ⁴¹ R. Tesch and P. M. Kowalski *Phys. Rev. B* **2022**, 105, 195153.
- ⁴² J. Wu, Y.-C. Wang, Y. Liu, B. Sun, Y. Zhao, J. Xian, X. Gao, H. Liu, and H. Song *Matter Radiat. at Extremes* **2022**, 7, 058402
- ⁴³ Y.-C. Wang and H. Jiang, *J. Chem. Phys.* **2019**, 150, 154116.
- ⁴⁴ K. Nawa, T. Akiyama, T. Ito, K. Nakamura, T. Oguchi and M. Weinert *Phys. Rev. B* **2018** 98, 035117.
- ⁴⁵ B. N. Harmon, V. P. Antropov, A. I. Lichtenstein, I. V. Solovyev, and V. I. Anisimov, *J. Phys. Chem. Solids* **1995** 56, 1521.
- ⁴⁶ S. K. Mohanta, S. N. Mishra, S. K. Srivastava and M. Rots, *Solid State Comm.* **2010** 150, 1789.
- ⁴⁷ I. L. M. Locht, Y. O. Kvashnin, D. C. M. Rodrigues, M. Pereiro, A. Bergman, L. Bergqvist, A. I. Lichtenstein, M. I. Katsnelson, A. Delin, A. B. Klautau, B. Johansson, I. Di Marco, and O. Eriksson, *Phys. Rev. B* **2016** 94, 085137.
- ⁴⁸ F. Nilsson, R. Sakuma, and F. Aryasetiawan, *Phys. Rev. B* **2013** 88, 125123.
- ⁴⁹ J.-B. Morée and B. Amadon, *Phys. Rev. B* **2018** 98, 205101.
- ⁵⁰ K. Tao, J. Zhou, Q. Sun, Q. Wang, V.S. Stepanyuk, and P. Jena, *Phys. Rev. B* **2014** 89, 085103.
- ⁵¹ G. Kresse and J. Hafner, *Phys. Rev. B* **1993** 47, 558.
- ⁵² G. Kresse and J. Furthmüller, *Phys. Rev. B* **1996** 54, 11169.
- ⁵³ F. Bultmark, F. Cricchio, O. Granas, and L. Nordstrom, *Phys. Rev. B* **2009** 80, 035121.
- ⁵⁴ F. Aryasetiawan, and O. Gunnarsson, *Rep. Prog. Phys.* **1998** 61, 237-312.
- ⁵⁵ F. Aryasetiawan, K. Karlsson, O. Jepsen, and U. Schönberger, *Phys. Rev. B* **2006** 74, 125106.
- ⁵⁶ T. Miyake, F. Aryasetiawan, and M. Imada, *Phys. Rev. B* **2009** 80, 155134.
- ⁵⁷ B. Amadon, and T. Applencour. *Phys. Rev. B* **2014** 89, 125110.
- ⁵⁸ N. Marzari and D. Vanderbilt, *Phys. Rev. B* **1997** 56, 12847.
- ⁵⁹ I. Souza, N. Marzari, and D. Vanderbilt, *Phys. Rev. B* **2001** 65, 035109.
- ⁶⁰ A. A. Mostofi, J. R. Yates, Y. -S. Lee, I. Souza, D. Vanderbilt, and N. Marzari, *Comput. Phys. Commun.* **2008** 178, 685.
- ⁶¹ P. E. Blochl, *Phys. Rev. B* **1994** 50, 17953.
- ⁶² H.J. Monkhorst, J.D. Pack, *Phys. Rev. B* **1976** 13, 5188-5192.
- ⁶³ K. Karlsson, F. Aryasetiawan and O. Jepsen *Phys. Rev. B* **2010** 81, 245113.
- ⁶⁴ V. Kashid, E. Şaşıoğlu, G. Bihlmayer, A. B. Shick, S. Blügel, arXiv preprint **2020** arXiv:2005.13901v1.
- ⁶⁵ B.I. Min, H.J.F. Jansen, T. Oguchi, and A.J. Freeman. *J. Magn. Mater.* **1986**, 61, 139-150.
- ⁶⁶ H. J. Kulik, M. Cococcioni, D. A. Scherlis, and N. Marzari. *Phys. Rev. L* **2006**, 97, 103001.